Passivated surface of high aluminum containing ZSM-5 by silicalite-1: synthesis and application in dehydration reaction

Girolamo Giordano, Massimo Migliori, Giorgia Ferrarelli, Gianfranco Giorgianni, Francesco Dalena, Peng Peng, Maxime Debost, Philippe Boullay, Zhen Liu, Hailing Guo, et al.

PASSIVATED SURFACE OF HIGH ALUMINUM CONTAINING ZSM-5 BY SILICALITE-1: SYNTHESIS AND APPLICATION IN DEHYDRATION REACTION

Girolamo GIORDANO[1], Massimo MIGLIORI[1,*], Giorgia FERRARELLI[2], Gianfranco GIORGIANNI[1], Francesco DALENA[1], Peng PENG[3,4], Maxime DEBOST[4,5], Philippe BOULLAY[5], Zhen LIU[3], Hailing GUO[3], Zi-Feng YAN[3], Svetlana MINTOVA[3,4]

[1] Laboratory of Catalysis and Industrial Chemistry, University of Calabria, Via P. Bucci – 87036 Rende (CS), Italy.

[2] Laboratory of Catalysis for Sustainable Production and Energy, University of Messina, Viale F. Stagno D'Alcontres 31 - 98165, Messina, Italy

[3] State Key Laboratory of Heavy Oil Processing, College of Chemical Engineering, China University of Petroleum (East China), Qingdao, Shandong 266580, China

[4] Laboratoire Catalyse et Spectrochimie (LCS), Normandie Université, ENSICAEN, UNICAEN, CNRS, 6 Boulevard Maréchal Juin, Caen, 14050, France

[5] Normandie Université, ENSICAEN, UNICAEN, CNRS, CRISMAT, 14000 Caen, France

*Corresponding author

E-mail address: massimo.migliori@unical.it; Phone: +39-0984-496641

ABSTRACT

Methanol dehydration reaction is an essential process to bridge the biomass conversion and chemicals. However, the undesired distribution of zeolite acidity hinders its excellent catalytic performance. In this work, the technique of passivating

surface acidity of a high aluminum containing ZSM-5 zeolite by the growth of Silicalite-1 layer under hydrothermal conditions is presented. The samples passivated with a single-step or double-step of Silicalite-1 deposition were tested for the dehydration of methanol to dimethyl ether and compared to the parent ZSM-5 zeolite using a bench-scale packed bed reactor operated at 160-240°C under atmospheric pressure. The conversion and selectivity for the single-step Silicalite-1 deposition catalyst decreased, and the amount of coke increased with respect to the parent ZSM-5 catalyst. The formation of an amorphous silica layer and the decrease of the active surface caused the drop in conversion and selectivity of the catalyst with the passivating single-step Silicalite-1 deposition with respect to the parent zeolite. In contrast, the double-step of Silicalite-1 deposition on the catalyst showed similar conversion to the parent ZSM-5 zeolite but an improved selectivity due to the low coke formation and retention in the highly porous structure.

Keywords: Surface Passivation; Zeolites; Methanol dehydration; Acidity control.

1. INTRODUCTION

In the past few decades, with the uncontrolled emission of greenhouse gases represented by CO_2, the world has been increasingly threatened by the issue of climate warming[1]. Controlling of the consumption of traditional fossil-based transportation fuels and chemicals is one of the main ways to reduce CO_2 emissions and achieve "carbon neutrality"[2,3]. Although transportation fuels may be gradually replaced by more sustainable energy sources like wind, solar and hydro technology, chemicals should still rely on carbon-based resources[4]. In this sense,

increasingly research attentions focus on the valorization and exploration of renewable carbon-based sources such as biomass to chemicals[3,5].

Methanol is an essential molecule for biomass conversion into chemicals[6]. On one hand, methanol can be easily manufactured via biomass gasification[7], and on the other hand, methanol can also be converted via dehydration to various chemicals such as dimethylether (DME) and light olefins[8]. For the latter process, zeolites (e. g. ZSM-5, SAPO-34, ZSM-22, ferrierite, etc.) play a dominant role due to the flexible and adjustable chemical composition (silicon-to-aluminum ratio), high hydrothermal stability and surface acidity[9,10]. However, the catalytic performance of the zeolites is always weakened by coke formation, which is chiefly due to the undesired nature, distribution and strength of the acid sites[11,12]. Therefore, it is of vital importance to find a solution towards improving the performance of zeolite catalysts by tuning their acidity in methanol dehydration process[13].

The main acidity of zeolites resides in the presence of Brønsted Acid Sites (BAS), however the hydrophobicity of the zeolite does not rely only on them and silanol networks play a crucial role in coke deposition being also more or less polar bonds [14]. This was recently highlighted in a study relating vapor adsorption capacities of water and methanol in zeolites to the hydroxyl concentration measured with ^{29}Si NMR and IR spectroscopy[15]. Thus, the passivation of zeolite surface is a promising way in tuning properties of already functional catalysts in the industry like ZSM-5 zeolites especially when polar molecules are involved.

To adjust the surface acidity and hydrophobicity, several techniques have been applied on several zeolites within "hybrid" (Red-Ox/Acid) catalyst toward improving their performance and stability for sustainable processes[16,17]. One

typical example is the epitaxial growth applied for passivation of zeolite surfaces, thus, to control the surface acidity and protect metallic sites promoting the coupling with the acid phase in a "hybrid catalysts"[18,19]. Enlighted by such an example, depositing a pure silica MFI zeolite (Silicalite-1) shell on the surface of the ZSM-5 zeolite core is a plausible way to passivate the undesired acidity within the ZSM-5 zeolite core[20–22] and to modify the acidity and tailor the catalysts' properties [23–28]. Moreover, various other techniques have been tested and described in literature to reach the goal of passivating surface acidity. Surface dealumination of a nano-sized ZSM-5 zeolite carried out before the organic template removal, allowed to prolong the lifetime of catalyst employed in the reaction of methanol to propylene [29]. Recently, it was also showed that reversing the external surface of ZSM-5 zeolite by positively charged hexadecyltrimethylammonium??? (HDTMA) allowed a selectively deposit of phosphorus on the external surface and pore entrance, thus leading to improved para-selectivity in the alkylation of toluene with methanol [30]. Additionally, chemical liquid deposition (CLD) and chemical vapor deposition (CVD) of TEOS have been successfully employed with the purpose of passivating surface acidity of zeolites [31–34].

The classical strategy for core-shell catalyst includes a two-step procedure, involving the core preparation and the shell growth; the coupling of Silicalite-1 on a ZSM-5 zeolite is the most used strategy. The thickness and morphology of Silicalite-1 shells are affected by the Si/Al ratio [20] and/or crystal size of the ZSM-5 core [21] and the coating procedure applied. The morphology of the core-shell

zeolites is also dependent on the silica sources and structure-directing agent (SDA) used for preparing the precursor mixtures [22].

Improved stability for ZSM-5/Silicalite-1 core-shell catalyst containing Mo in methane de-hydro-aromatization was reported; the core-shell catalyst exhibited an excellent shape selectivity without lowering the conversion significantly as a consequence of the reduced acidity [35]. The advantage of tuning the surface acidity of the core-shell catalysts in methanol-to-hydrocarbon reactions and pyrolysis was reported as well [36,3738]. Other examples for ZSM-5 zeolites coated with a layer of Silicalite-1 were reported and employed in various applications[39] such as methanol conversion into gasoline and diesel[39] , ketonization and cracking reactions[40] and alkylation of toluene[20–22,41,42]. However, the Si/Al ratio in ZSM-5 core used was relatively high, ranging from 25 to more than 100, which hinders to broaden the application of the core-shell catalyst is the acidity of the zeolitic core.

In this paper, we report the preparation of novel catalysts with a ZSM-5 core with a low Si/Al ratio passivated with a single and multi-layer Silicalite-1. The novel catalysts with high aluminum content of the core and high number of external acid sites were tested in methanol dehydration reaction.

2. EXPERIMENTAL

2.1 Preparation of Core-Shell Zeolite Catalysts

A ZSM-5 zeolite (Si/Al=11 in the gel) was prepared under hydrothermal conditions[43] starting from a gel with the following molar composition: 0.08 Na_2O-0.08 TPABr–0.045Al_2O3–1 SiO_2–20 H_2O. Briefly 0,56 g of sodium hydroxide (NaOH), 2,82 g of sodium aluminate ($NaAlO_2$) and 7.1 g of tetrapropylammonium

bromide (TPABr) were dissolved in 119.6 g of distilled water. Finally, 20 g of precipitated silica (ADD TYPE ???) was added. The resultant gel was stirred for 1 h at room temperature, then transferred in a PTFE-lined stainless-steel autoclave and kept in a static oven at 170°C for 7 days. The obtained sample was washed with distillate water and calcinated at 550°C to eliminate the structural organic template (SDA). The acidic form of the samples was obtained after two cycles (2 h each at 80°C) of ionic exchange with NH_4Cl (1 M) and a subsequent calcination at 550°C. The parent zeolite catalyst labeled as ZSM-5_P was also used as a starting material for the following passivation treatments with Silicalite-1.

Two catalysts with passivated surface acidity were synthesized by growth of Sillicalite-1 on the parent zeolite sample (ZSM-5_P) using a single-step or double-step deposition. 5 g of ZSM-5 crystals in H^+-form were immersed in 10 g of Silicalite-1 precursor mixture prepared by mixing tetraethyl orthosilicate (TEOS), tetrapropylammonium hydroxide (TPAOH), and deionized water. The precursor mixture with the following molar was obtained: 2 SiO_2: 0.5 TPAOH: 8 EtOH: 120 H_2O [21]. The hydrothermal synthesis was performed at 180°C for 24h using a tumbling oven, and the as-prepared materials after purification was calcined at 550°C (ramp: 2°C/min, duration time: 8 h, condition: static air) (named as single-Silicalite-1 deposition step catalyst: ZSM-5_X). After purification and calcination, a part of ZSM-5_X crystals was used to repeat the synthesis of the Silicalite-1 shell, in a new synthesis gel, in order to increase the Silicalite-1 thickness and to obtain a better passivation performance (named as double-Silicalite-1 deposition step catalyst ZSM-5_XX).

2.2 Characterization of the catalysts

The crystallinity of the samples was determined by a Miniflex600 (Rigaku, Japan) diffractometer (λ_{Cu} = 1.540560 Å, 40 kV, 15 mA); the X-ray diffraction patterns were recorded in the 2θ range 5-40° (step: 0.01°; scanning rate: 1°/min).

The chemical composition of the samples was characterized using a GBC 932AA atomic absorption spectrometer (AAS, GCB Scientific Equipment, Australia).

Electron microscopy imaging and Energy Dispersive X-Ray Spectroscopy (EDS) were performed using a JEOL F200 transmission electron microscope (TEM) operated at 200kV equipped with a Gatan RIO16 camera and a JEOL Centurio EDS detector.

The N_2 physisorption measurements of the samples were carried out using an ASAP 2020 porosimeter (Micromeritics, USA) at 77 K. Specific surface areas and micropore volumes were calculated using the BET and t-plot methods, respectively[44].

NH_3 temperature-programmed desorption measurements (NH_3-TPD) of zeolites[45] were performed by a TPDRO1100 (Thermo Scientific, USA) equipped with a TCD detector, according to the following procedure. 100 mg of dried sample were loaded in a linear quartz micro-reactor (i.d., 4 mm; l., 200 mm) and pre-treated at 300 °C in helium flow of 20 ml/min. Then temperature was lowered to 150 °C and the sample was saturated with a stream of NH_3/He (10% v/v) flowing at 20 ml/min for 120 minutes. Afterward, physisorbed ammonia was removed at 150 °C using a helium flow until TCD-signal baseline stabilization. Ammonia desorption measurement was carried out in the temperature range of 100–700 °C with a heating rate of 10 °C/min using a helium flow rate of 20 ml/min.

The IR spectra of the samples were recorded using a Nicolet iS 10 FTIR spectrometer (Thermo Scientific, USA) equipped with a DTGS detector. The self-supported samples (25 mg, disk) were initially outgassed at 10^{-5} torr under heating (400°C for 2h, heating rate of 10 °C/min), and the spectra before and after pyridine (Py) delivery were recorded. FTIR spectra were measured at room temperature (r.t.) and 10^{-5}-10^{-4} Torr in the mid-infrared region (MIR: 4000-400 cm^{-1}), with an optical resolution of $4cm^{-1}$ [46,47]. The physisorbed Py was removed under degassing of the sample at 150°C and 10^{-5} Torr for 60min before spectrum acquisition[48] . The concentration of the Brønsted and Lewis acid sites was calculated via integration of the peaks at 1545 cm^{-1} and ⍰1454 cm^{-1}, respectively [49,50]. The measurement was performed on three independent samples and data were reported as an average standard deviation.

2.3 Catalytic tests

140 mg of catalysts (pellet, 300-500μm) were tested in a U-shaped quartz packed bed reactor (ID = 15mm, L = 40mm) at 140-240°C and atmospheric pressure with a weight hourly space velocity (WHSV) of $4g_{MeOH}\cdot(g_{cat}\cdot h)^{-1}$ using a mixture of methanol (0.06 mol/mol) and nitrogen as carrier (60 STP ml/min)[51], after 2h pretreatment at 240°C in N_2 flow. Temperature and time for the pretreatment of the samples were established based on the TG results for the catalysts in H^+ form; the temperature for removal of water was identified.

A GC-FID (Agilent 7890 A) equipped with a J&W 125-1032 column was used to measure the products [51]. Methanol conversion (ε_{MeOH}) and DME selectivity (S_{DME})

were calculated according to eq. 1 and 2, considering methanol (*MeOH*) and DME molar flow rate entering (*in*) or leaving the reactor (*out*):

$$\varepsilon_{MeOH} = \frac{\dot{n}_{MeOH_{in}} - \dot{n}_{MeOH_{out}}}{\dot{n}_{MeOH_{in}}} \quad (1)$$

$$S_{DME} = \frac{2\,\dot{n}_{DME_{out}}}{\dot{n}_{MeOH_{in}} - \dot{n}_{MeOH_{out}}} \quad (2)$$

2.4 Coke Analysis

The amount of deposited coke on the used catalysts was measured by thermo-gravimetric analysis (TGA) using a TA Instruments SDT 650; the weight loss in the range 250-850°C (heating rate 10°C/min) was measured [12]. The soluble coke species were detected via GC-MS (Agilent 7820A, MSD 5977E) analysis. Prior to the test, HF (40%) was used for dissolving the spent catalysts; then, dichloromethane was used as organic phase to extract the coke species [51].

3. RESULTS AND DISCUSSION

3.1 Physical and chemical properties of samples

The X-ray patterns of the parent ZSM-5 and passivated catalysts contain the characteristic Bragg peaks for the MFI type zeolites (**Figure 1**); no other phases were observed. The intensity of the (120) and (053) peaks at 9.851 and 29.904° 2Theta slightly decreased for the samples with passivated surface acidity. Conversely, the intensity of the (011) peak at 7.935° slightly increased. The latter observation might indicate a preferential growth of the Silicalite-1 on the (011) plane. Conversely, the intensity of the (120) and (053) peaks decreased, which is in line with the formation of an amorphous silica shell on the surface of the parent ZSM-5 zeolite.

FIGURE 1 HERE

The chemical composition of the samples is summarized in **Table 1;** the Si/Al ratio increases with the increasing of Silicalite-1 layer thickness. The amount of Silicalite-1 shell was estimated to be 12 wt. % and 31 wt. % in the single and double- deposition step of Silicalite-1, respectively [52]. The AA analyses were also performed of the mother liquor after the solid separation and in all cases, the presence of aluminum was not detected.

TABLE 1 HERE

All samples present a mixed Type I/IV isotherms with H4 hysteresis at 0.45 P/P^0 (**Figure 2**), typical of aggregated crystals containing textural mesopores [44]. The parent zeolite ZSM-5_P showed similar porosity to other MFI zeolites reported before [53]. The BET surface area (S_{BET}) of the ZSM-5_X sample decreased by 14 %, with respect to the parent sample (**Table 1**), which is in line with other published results[54].

FIGURE 2 HERE

A similar trend was observed for the microporous area (S_{micro}) and external surface area (S_{ext}) of ZSM-5_X. BET surface area (S_{BET}), microporous area (S_{micro}) and external surface area (S_{ext}) of double-Silicalite-1 deposited sample ZSM-5_XX was higher than that of the sample with only one Silicalite-1 deposition step.

TEM observations of the of the parent ZSM-5 sample reveal a bimodal particle size distribution. Two types of agglomerates are observed, consisting, on the one hand, of crystals of 100 nm maximum (**Figure 3A**) and, on the other hand, of larger crystals in the form of rods (thickness greater than 200 nm and length greater than

1 micrometer). In both cases, the shape of the crystals is well defined, and their surface is free of any coating (**Figure 3B**).

After the first passivation step, it is possible to observe the presence of amorphous material surrounding the two types of agglomerates (**Figure 4A**). Individually, the surface of the crystals is also covered, at least partially, by a thin amorphous layer (**Figure 4B**).

FIGURE 4 HERE

After the second passivation step, the ZSM-5 surface is covered by a thicker layer (**Figure 5A**). Within this layer, crystalline domains representative for MFI type zeolites can be seen (**Figure 5B**).

FIGURE 5 HERE

The NH_3-TPD profiles of the samples (**Figure 6**) exhibit peaks at different temperatures: (*l*) is the low temperature peak (i.e. below 300°C), (*m*) is the medium temperature peak (below 500°C) and two peaks are also present at temperature higher than 550°C. In order to assess the acidity of the samples, due to the partial overlapping of the peaks, all of them were considered for the overall curve deconvolution. Moreover, since the peaks at temperature above 550°C are most likely associated with silanols dihydroxylation[55], their contribution was not included in the total acidity determination (**Table 2**). The NH_3 adsorption of the ZSM-5_X sample in comparison to the parent ZSM-5_P decreased by 26%, and this is in agreement with the evidence of the formation of an amorphous silica layer on the core [54] even though no detectable in the XRD, reducing the accessibility of the structure by the probe molecule. Furthermore, the total NH_3 adsorption measured for the double-Silicalite-1 deposited (ZSM-5_XX) zeolite is lower than that of the

parent ZSM-5_P but higher than that of the ZSM-5_X sample. A similar trend was observed for the medium temperature peak (*m*), and the (*l*) and (*h*) peaks decreased for the samples after a single and double Silicalite-1 deposition step (**Table 2**).

FIGURE 6 HERE

TABLE 2 HERE

The FT-IR spectra of the parent and catalysts with passivated surface acidity using Pyridine (**Figure 7**) indicate a stepwise decrease of the Brønsted and Lewis acidity for both ZSM-5_X and ZSM-5_XX samples, which correlate linearly with the Si/Al ration of the catalysts (**Table 2**). The pyridine was used as a probe molecule, and the spectra were recorded after treatment of the samples at 150°C [48]. The FT-IR results for samples ZSM-5_P and ZSM-5_X are in line with the NH_3-TPD results whilst 23% difference was found for sample ZSM-5_XX. This difference could be probably due to the different size of the probes used, i.e., pyridine being larger failed to reach all acid sites. This result are in agreement with previous reports[54] and a good linear correlation (see Supplementary Information) between the Al content (**Table 1**) and acidity the of the catalyst from FT-IR is found. Therefore, the data from the Pyridine adsorption measurements were used in the discussion.

FIGURE 7 HERE

3.2 Catalytic tests

The methanol conversion for all catalysts was found to be improved with raising the temperature from 140 to 240°C, approaching the equilibrium at 240 °C (**Figure 8**). The parent catalyst ZSM-5_P showed the highest conversion at all temperatures. This is attributed to the highest acidity of the parent ZSM-5_P

catalyst. While the single-Silicalite-1 deposited sample (sample ZSM-5_X) with similar acidity to the parent catalyst according to the FTIR showed lower conversion in the entire temperature range. The double-Silicalite-1 deposited catalyst (sample ZSM-5-XX) favorably impacts the methanol conversion compared to the ZSM-5_X sample, although the acidity was markedly reduced.

FIGURE 8 HERE

The selectivity was equal to 1 for all samples in the range 160-200°C. At 220 and 240°C, the double-Silicalite-1 deposited catalyst (ZSM-5_XX) exhibited the highest selectivity of 98.4 and 96.9 %, respectively; a more pronounced decrease of the selectivity was detected for the single Silicalite-1 layered catalyst (ZSM-5-X). It seems that the observed trends in the conversion and selectivity are not in accordance with the acidity of the catalysts and are more dependent on their textural properties. Compared to the ZSM-5_P and ZSM-5_XX catalysts, the BET surface area, micropore area, and external surface areas are decreased for ZSM-5_X catalyst. This sample also showed higher silica content according to the chemical analysis and the arrangement of this layer in form of an amorphous silica shell was supported by the partial decrease of the Bragg peaks with (hkl) of (120) and (053) (**Figure 1**). Therefore, the reduced conversion for ZSM-5_X could be attributed to the surface properties of the samples; the amorphous silica shell partially blocked the ZSM-5_X and was restored after the growth of the second shell. The lower selectivity showed by the ZSM-5_X catalyst, with respect to the ZSM-5_P and ZSM-5_XX catalysts, could indicate the increased pore tortuosity at the pore mouth, induced by the presence of amorphous silica, leading to an enhanced residence time of the formed DME within the micropores, in the presence of acidic sites, and

also to the formation of olefins. This is confirmed by the detection of C_2-C_3 olefins as a function of temperature, as presented in **Figure 9**.

FIGURE 9 HERE

It clearly appears that no olefin signal was detected at temperatures lower than 220°C, whilst the ZSM-5_X promoted more olefins than the parent ZSM-5_P catalyst. On the contrary, this effect was significantly reduced in the case of the double-Silicalite-1 deposited catalyst (ZSM-5_XX), which is in accordance with the recovered textural properties of the sample and reduced acidity.

Another interesting observation is the acid sites efficiency based on the average/apparent Turn Over Frequency (TOF), calculated far from the equilibrium conditions at 160° and 180°C (**Figure 10**):

$$\mathbf{TOF}\ [\boldsymbol{s^{-1}}] = \frac{(\mathbf{WHSV/3600/MW}_{\boldsymbol{MeOH}})\cdot \mathbf{x}_{\boldsymbol{MeOH}}}{\mathbf{Bronsted\ AS}} \quad (3)$$

where the ratio $WHSV/MW_{MeOH}$ is the MeOH hourly molar flow rate per gram of catalyst [$\mu mol\cdot(gc_{at}\cdot h)^{-1}$], x_{MeOH} is the observed MeOH conversion, and total AS is the Brønsted acid sites concentration ($\mu mol\cdot g_{cat}^{-1}$) determined from FTIR data (**Table 2**). The Brønsted acid sites are of vital importance in dehydration reactions.

FIGURE 10 HERE

In summary, the double-Silicalite-1 deposited catalyst (ZSM-5_XX) showed the best performance in terms of acid sites efficiency in comparison to the parent ZSM-5_P and single- Silicalite-1 deposited catalyst ZSM-5_X at 180°C.

3.3 Coke Analysis

TGA analyses were performed on used parent and catalysts covered with Silicalite-1 after 5 h reaction. The DTG curves contain two broad peaks at 321-

357°C (low-temperature region, LT) and at 549-563°C (high-temperature region, HT), indicating the presence of coke on the spent catalysts [51]. The spent single-Silicalite-1 deposited catalyst (ZSM_5_X) showed the highest coke formation (**Table 3**), while the spent double-Silicalite-1 deposited catalyst (ZSM-5_XX) contained the lowest amount of coke.

TABLE 3 HERE

GC-MS analysis of the coke species extracted from the spent parent, and catalysts with passivated surface acidity revealed the presence of pentamethyl benzene and hexamethyl benzene (**Figure 11**), which are the typical coke species found on the external surface of spent catalyst used for the dehydration of methanol to DME [12].

FIGURE 11 HERE

The area of the peaks associated with pentamethyl-benzene and hexamethyl-benzene (**Figure 11**) correlated well with the total weight loss determined by TGA (correlation not shown), thus suggesting that the weight loss could be related to the soluble coke species coherent with the relatively low reaction temperatures. Moreover, the ZSM-5_X catalyst has shown the presence of 1,2,4,5-tetramethylbenzene, while the latter was not shown for the ZSM-5_P and ZSM-5_XX catalysts, in line with the assumed increased tortuosity for the ZSM-5_X sample.

4. CONCLUSIONS

The goal of passivating the surface acidity of a high Al containing ZSM-5 zeolite by single- and double-layer Silicalite-1 deposition step has been successfully

achieved. The obtained samples were used for the reaction of methanol dehydration to DME. Compared to the parent ZSM-5 zeolite, the conversion and selectivity of the single-Silicalite-1 layered catalyst were found to decrease while the amount of coke increased with respect to the uncovered ZSM-5. The formation of an amorphous silica layer after the first growth cycle ended up in a low conversion and selectivity of the ZSM-5_X catalyst. On the contrary, catalytic results demonstrated that depositing a second of Silicalite-1 layer could positively contribute to the catalyst performance. Reduction in surface acidity, mainly responsible for coke formation, improved the catalyst efficiency with significant reduction of coke formation, mainly poly-methyl benzenes, on the external surface of the spent catalysts. In addition, calculation of Turn Over Frequency, calculated using Brønsted acid sites, confirmed a comparable efficiency of the double-layered passivated catalysts and the parent zeolite.

ACKNOWLEDGMENTS

Authors gratefully acknowledge the “Ministero degli Affari Esteri e della Cooperazione Internazionale” (MAECI) of Italy and “Ministry of Science and Technology of the People's Republic of China” (MOST) for the financial support of project “B2CLIF - Biowaste to Chemicals and LIquid Fuels”, cofunded in the framework of a bilateral agreement between MAECI and MOST.

REFERENCES

(1) Peters, G. P.; Andrew, R. M.; Canadell, J. G.; Friedlingstein, P.; Jackson, R. B.; Korsbakken, J. I.; Le Quéré, C.; Peregon, A. Carbon Dioxide Emissions Continue to Grow amidst Slowly Emerging Climate Policies. *Nat. Clim. Chang.* **2020**, *10* (1), 3–6. https://doi.org/10.1038/s41558-019-0659-6.

(2) Peter, S. C. Reduction of CO2 to Chemicals and Fuels: A Solution to Global Warming and Energy Crisis. *ACS Energy Lett.* **2018**, *3* (7), 1557–1561. https://doi.org/10.1021/acsenergylett.8b00878.

(3) Shahid, M. K.; Batool, A.; Kashif, A.; Nawaz, M. H.; Aslam, M.; Iqbal, N.; Choi, Y. Biofuels and Biorefineries: Development, Application and Future Perspectives Emphasizing the Environmental and Economic Aspects. *J. Environ. Manage.* **2021**, *297*, 113268. https://doi.org/https://doi.org/10.1016/j.jenvman.2021.113268.

(4) Ennaert, T.; Van Aelst, J.; Dijkmans, J.; De Clercq, R.; Schutyser, W.; Dusselier, M.; Verboekend, D.; Sels, B. F. Potential and Challenges of Zeolite Chemistry in the Catalytic Conversion of Biomass. *Chem. Soc. Rev.* **2016**, *45* (3), 584–611. https://doi.org/10.1039/C5CS00859J.

(5) Taarning, E.; Osmundsen, C. M.; Yang, X.; Voss, B.; Andersen, S. I.; Christensen, C. H. Zeolite-Catalyzed Biomass Conversion to Fuels and Chemicals. *Energy Environ. Sci.* **2011**, *4* (3), 793–804. https://doi.org/10.1039/C004518G.

(6) Li, Y.; Li, Y.; Zhang, X.; Wang, C.; Li, X.; Ma, L. Exergy Analysis of Renewable Light Olefin Production System via Biomass Gasification and Methanol Synthesis. *Int. J. Hydrogen Energy* **2021**, *46* (5), 3669–3683.

https://doi.org/https://doi.org/10.1016/j.ijhydene.2020.10.213.

(7) Santos, R. G. dos; Alencar, A. C. Biomass-Derived Syngas Production via Gasification Process and Its Catalytic Conversion into Fuels by Fischer Tropsch Synthesis: A Review. *Int. J. Hydrogen Energy* **2020**, *45* (36), 18114–18132. https://doi.org/https://doi.org/10.1016/j.ijhydene.2019.07.133.

(8) Tian, P.; Wei, Y.; Ye, M.; Liu, Z. Methanol to Olefins (MTO): From Fundamentals to Commercialization. *ACS Catalysis*. 2015. https://doi.org/10.1021/acscatal.5b00007.

(9) Li, J.; Wei, Y.; Liu, G.; Qi, Y.; Tian, P.; Li, B.; He, Y.; Liu, Z. Comparative Study of MTO Conversion over SAPO-34, H-ZSM-5 and H-ZSM-22: Correlating Catalytic Performance and Reaction Mechanism to Zeolite Topology. *Catal. Today* **2011**, *171* (1), 221–228. https://doi.org/https://doi.org/10.1016/j.cattod.2011.02.027.

(10) Catizzone, E.; Migliori, M.; Mineva, T.; van Daele, S.; Valtchev, V.; Giordano, G. New Synthesis Routes and Catalytic Applications of Ferrierite Crystals. Part 2: The Effect of OSDA Type on Zeolite Properties and Catalysis. *Microporous Mesoporous Mater.* **2020**, *296*, 109988. https://doi.org/https://doi.org/10.1016/j.micromeso.2019.109988.

(11) Catizzone, E.; Daele, S. Van; Bianco, M.; Di Michele, A.; Aloise, A.; Migliori, M.; Valtchev, V.; Giordano, G. Catalytic Application of Ferrierite Nanocrystals in Vapour-Phase Dehydration of Methanol to Dimethyl Ether. *Appl. Catal. B Environ.* **2019**, *243*, 273–282. https://doi.org/https://doi.org/10.1016/j.apcatb.2018.10.060.

(12) Migliori, M.; Catizzone, E.; Aloise, A.; Bonura, G.; Gómez-Hortigüela, L.;

Frusteri, L.; Cannilla, C.; Frusteri, F.; Giordano, G. New Insights about Coke Deposition in Methanol-to-DME Reaction over MOR-, MFI- and FER-Type Zeolites. *J. Ind. Eng. Chem.* **2018**, *68*, 196–208. https://doi.org/10.1016/j.jiec.2018.07.046.

(13) Busca, G. Acid Catalysts in Industrial Hydrocarbon Chemistry. *Chem. Rev.* **2007**, *107* (11), 5366–5410. https://doi.org/10.1021/cr068042e.

(14) Medeiros-Costa, I. C.; Dib, E.; Nesterenko, N.; Dath, J.-P.; Gilson, J.-P.; Mintova, S. Silanol Defect Engineering and Healing in Zeolites: Opportunities to Fine-Tune Their Properties and Performances. *Chem. Soc. Rev.* **2021**, *50* (19), 11156–11179. https://doi.org/10.1039/d1cs00395j.

(15) Lions, M.; Daniel, C.; Coasne, B.; Meunier, F.; Tuel, A.; Farrusseng, D. The Pivotal Role of Critical Hydroxyl Concentration in Si-Rich Zeolites for Switching Vapor Adsorption. **2021**.

(16) Li, Y.; Li, L.; Yu, J. Applications of Zeolites in Sustainable Chemistry. *Chem* **2017**, *3* (6), 928–949. https://doi.org/10.1016/j.chempr.2017.10.009.

(17) Bonura, G.; Cannilla, C.; Frusteri, L.; Catizzone, E.; Todaro, S.; Migliori, M.; Giordano, G.; Frusteri, F. Interaction Effects between CuO-ZnO-ZrO2 Methanol Phase and Zeolite Surface Affecting Stability of Hybrid Systems during One-Step CO2 Hydrogenation to DME. *Catal. Today* **2020**, *345*, 175–182. https://doi.org/10.1016/j.cattod.2019.08.014.

(18) Wu, Y.; Chai, Y.; Li, J.; Guo, H.; Wen, L.; Liu, C. Preparation of Silicalite-1@Pt/Alumina Core-Shell Catalyst for Shape-Selective Hydrogenation of Xylene Isomers. *Catal. Commun.* **2015**, *64*, 110–113. https://doi.org/10.1016/j.catcom.2015.02.004.

(19) Yang, G.; Wang, D.; Yoneyama, Y.; Tan, Y.; Tsubaki, N. Facile Synthesis of H-Type Zeolite Shell on a Silica Substrate for Tandem Catalysis. *Chem. Commun.* **2012**, *48* (9), 1263–1265. https://doi.org/10.1039/c2cc16713a.

(20) Van Vu, D.; Miyamoto, M.; Nishiyama, N.; Egashira, Y.; Ueyama, K. Selective Formation of Para-Xylene over H-ZSM-5 Coated with Polycrystalline Silicalite Crystals. *J. Catal.* **2006**, *243* (2), 389–394. https://doi.org/10.1016/j.jcat.2006.07.028.

(21) Vu, D. Van; Miyamoto, M.; Nishiyama, N.; Ichikawa, S.; Egashira, Y.; Ueyama, K. Catalytic Activities and Structures of Silicalite-1/H-ZSM-5 Zeolite Composites. *Microporous Mesoporous Mater.* **2008**, *115* (1–2), 106–112. https://doi.org/10.1016/j.micromeso.2007.12.034.

(22) Van Vu, D.; Miyamoto, M.; Nishiyama, N.; Egashira, Y.; Ueyama, K. Morphology Control of Silicalite/HZSM-5 Composite Catalysts for the Formation of Para-Xylene. *Catal. Letters* **2009**, *127* (3–4), 233–238. https://doi.org/10.1007/s10562-008-9676-1.

(23) Li, X.; Rezaei, F.; Ludlow, D. K.; Rownaghi, A. A. Synthesis of SAPO-34@ZSM-5 and SAPO-34@Silicalite-1 Core-Shell Zeolite Composites for Ethanol Dehydration. *Ind. Eng. Chem. Res.* **2018**, *57* (5), 1446–1453. https://doi.org/10.1021/acs.iecr.7b05075.

(24) Bouizi, Y.; Majano, G.; Mintova, S.; Valtchev, V. Beads Comprising a Hierarchical Porous Core and a Microporous Shell. *J. Phys. Chem. C* **2007**, *111* (12), 4535–4542. https://doi.org/10.1021/jp068240+.

(25) Fan, Y.; Lei, D.; Shi, G.; Bao, X. Synthesis of ZSM-5/SAPO-11 Composite and Its Application in FCC Gasoline Hydro-Upgrading Catalyst. *Catal. Today* **2006**,

114 (4 SPEC. ISS.), 388–396. https://doi.org/10.1016/j.cattod.2006.02.050.

(26) Zheng, J.; Wang, G.; Pan, M.; Guo, D.; Zhao, Q.; Li, B.; Li, R. Hierarchical Core-Shell Zeolite Composite ZSM-5@SAPO-34 Fabricated by Using ZSM-5 as the Nutrients for the Growth of SAPO-34. *Microporous Mesoporous Mater.* **2015**, *206* (C), 114–120. https://doi.org/10.1016/j.micromeso.2014.12.011.

(27) Zhang, L.; Jiang, Z. X.; Yu, Y.; Sun, C. S.; Wang, Y. J.; Wang, H. Y. Synthesis of Core-Shell ZSM-5@meso-SAPO-34 Composite and Its Application in Methanol to Aromatics. *RSC Adv.* **2015**, *5* (69), 55825–55831. https://doi.org/10.1039/c5ra10296k.

(28) Razavian, M.; Fatemi, S. Synthesis and Application of ZSM-5/SAPO-34 and SAPO-34/ZSM-5 Composite Systems for Propylene Yield Enhancement in Propane Dehydrogenation Process. *Microporous Mesoporous Mater.* **2015**, *201* (C), 176–189. https://doi.org/10.1016/j.micromeso.2014.09.022.

(29) Feng, R.; Yan, X.; Hu, X.; Yan, Z.; Lin, J.; Li, Z.; Hou, K.; Rood, M. J. Surface Dealumination of Micro-Sized ZSM-5 for Improving Propylene Selectivity and Catalyst Lifetime in Methanol to Propylene (MTP) Reaction. *Catal. Commun.* **2018**, *109* (January), 1–5. https://doi.org/10.1016/j.catcom.2018.02.005.

(30) Yi, D.; Meng, X.; Xu, X.; Liu, N.; Shi, L. Catalytic Performance of Modified ZSM-5 Designed with Selectively Passivated External Surface Acidity by Phosphorus. *Ind. Eng. Chem. Res.* **2019**, *58* (24), 10154–10163. https://doi.org/10.1021/acs.iecr.9b00629.

(31) Mesa, S.; Arboleda, J.; Echavarría, A.; López-Suárez, F. E. Ferrierite Zeolite Passivation and Its Catalytic Application in Toluene Disproportionation.

Chem. Eng. Sci. **2019**, *208*, 115147. https://doi.org/10.1016/j.ces.2019.08.005.

(32) Zhu, Z.; Chen, Q.; Xie, Z.; Yang, W.; Kong, D.; Li, C. Shape-Selective Disproportionation of Ethylbenzene to Para-Diethylbenzene over ZSM-5 Modified by Chemical Liquid Deposition and MgO. *J. Mol. Catal. A Chem.* **2006**, *248* (1–2), 152–158. https://doi.org/10.1016/j.molcata.2005.10.023.

(33) Lv, J.; Hua, Z.; Zhou, J.; Liu, Z.; Guo, H.; Shi, J. Surface-Passivated Hierarchically Structured ZSM5 Zeolites: High-Performance Shape-Selective Catalysts for Para-Xylene Production. *ChemCatChem* **2018**, *10* (10), 2278–2284. https://doi.org/10.1002/cctc.201800044.

(34) Losch, P.; Boltz, M.; Bernardon, C.; Louis, B.; Palčić, A.; Valtchev, V. Impact of External Surface Passivation of Nano-ZSM-5 Zeolites in the Methanol-to-Olefins Reaction. *Appl. Catal. A Gen.* **2016**, *509*, 30–37. https://doi.org/10.1016/j.apcata.2015.09.037.

(35) Jin, Z.; Liu, S.; Qin, L.; Liu, Z.; Wang, Y.; Xie, Z.; Wang, X. Methane Dehydroaromatization by Mo-Supported MFI-Type Zeolite with Core-Shell Structure. *Appl. Catal. A Gen.* **2013**, *453*, 295–301. https://doi.org/10.1016/j.apcata.2012.12.043.

(36) Goodarzi, F.; Herrero, I. P.; Kalantzopoulos, G. N.; Svelle, S.; Lazzarini, A.; Beato, P.; Olsbye, U.; Kegnæs, S. Synthesis of Mesoporous ZSM-5 Zeolite Encapsulated in an Ultrathin Protective Shell of Silicalite-1 for MTH Conversion. *Microporous Mesoporous Mater.* **2020**, *292* (July 2019), 109730. https://doi.org/10.1016/j.micromeso.2019.109730.

(37) Li, M.; Hu, Y.; Fang, Y.; Tan, T. Coating Mesoporous ZSM-5 by Thin

Microporous Silicalite-1 Shell: Formation of Core/Shell Structure, Improved Hydrothermal Stability and Outstanding Catalytic Performance. *Catal. Today* **2020**, *339*, 312–320. https://doi.org/10.1016/j.cattod.2019.02.041.

(38) Feng, X. B.; Cao, J. P.; Yao, N. Y.; He, Z. M.; Zhang, L. Y.; Liu, T. L.; Zhao, X. Y.; Gao, X. H. Simultaneous Enhancement of Aromatic Products and Catalytic Lifetime for Catalytic Re-Forming of Lignite Pyrolysis Volatiles over a Self-Assembled Hierarchical Core-Shell ZSM-5@Silicalite-1 Zeolite. *ACS Sustain. Chem. Eng.* **2021**, *9* (38), 12960–12969. https://doi.org/10.1021/acssuschemeng.1c04439.

(39) Zheng, J.; Sun, X.; Du, Y.; Qin, B.; Zhang, Y.; Zhang, H.; Pan, M.; Li, R. Structural Features of Core–Shell Zeolite–Zeolite Composite and Its Performance for Methanol Conversion into Gasoline and Diesel. *J. Mater. Res.* **2016**, *31* (15), 2302–2316. https://doi.org/10.1557/jmr.2016.208.

(40) Ghorbanpour, Arian Gumidyala,Abhishek Grabow,Lars C. Crossley, S. P. an. J. D. R. Epitaxial Growth of ZSM-5 @ Silicalite-1 : Passivated Surface Acidity. **2015**, No. 4, 4006–4016.

(41) Deng, Y. Q.; Zhou, W. F.; Lv, H. M.; Zhang, Y. Y.; Au, C. T.; Yin, S. F.; Deng; Deng, Y. Q.; Zhou, W. F.; Lv, H. M.; Zhang, Y. Y.; Au, C. T.; Yin, S. F. Synthesis of HZSM-5@silicalite-1 Core-Shell Composite and Its Catalytic Application in the Generation of p-Xylene by Methylation of Toluene with Methyl Bromide. *RSC Adv.* **2014**, *4* (70), 37296–37301. https://doi.org/10.1039/c4ra04126g.

(42) Li, G.; Wu, C.; Dong, P.; Ji, D.; Zhang, Y. Core–Shell HZSM-5@silicalite-1 Composite: Controllable Synthesis and Catalytic Performance in Alkylation of Toluene with Methanol. *Catal. Letters* **2020**, No. 0123456789.

https://doi.org/10.1007/s10562-019-03085-y.

(43) Migliori, M.; Aloise, A.; Giordano, G. Methanol to Dimethylether on H-MFI Catalyst: The Influence of the Si/Al Ratio on Kinetic Parameters. *Catal. Today* **2014**, *227*, 138–143. https://doi.org/10.1016/j.cattod.2013.09.033.

(44) Thommes, M.; Kaneko, K.; Neimark, A. V.; Olivier, J. P.; Rodriguez-Reinoso, F.; Rouquerol, J.; Sing, K. S. W. Physisorption of Gases, with Special Reference to the Evaluation of Surface Area and Pore Size Distribution (IUPAC Technical Report). *Pure Appl. Chem.* **2015**, *87* (9–10), 1052–1069. https://doi.org/10.1515/pac-2014-1117.

(45) Catizzone, E.; Aloise, A.; Migliori, M.; Giordano, G. The Effect of FER Zeolite Acid Sites in Methanol-to-Dimethyl-Ether Catalytic Dehydration. *J. Energy Chem.* **2017**, *26* (3), 406–415. https://doi.org/10.1016/j.jechem.2016.12.005.

(46) Busca, G. Acidity and Basicity of Zeolites: A Fundamental Approach. *Microporous Mesoporous Mater.* **2017**, *254* (June 2016), 3–16. https://doi.org/10.1016/j.micromeso.2017.04.007.

(47) Phung, T. K.; Busca, G. On the Lewis Acidity of Protonic Zeolites. *Appl. Catal. A Gen.* **2015**, *504*, 151–157. https://doi.org/10.1016/j.apcata.2014.11.031.

(48) Zholobenko, V.; Freitas, C.; Jendrlin, M.; Bazin, P.; Travert, A.; Thibault-Starzyk, F. Probing the Acid Sites of Zeolites with Pyridine: Quantitative AGIR Measurements of the Molar Absorption Coefficients. *J. Catal.* **2020**, *385*, 52–60. https://doi.org/10.1016/j.jcat.2020.03.003.

(49) Gould, N. S.; Xu, B. Quantification of Acid Site Densities on Zeolites in the Presence of Solvents via Determination of Extinction Coefficients of

Adsorbed Pyridine. *J. Catal.* **2018**, *358*, 80–88. https://doi.org/10.1016/j.jcat.2017.11.016.

(50) Bordiga, S.; Lamberti, C.; Bonino, F.; Travert, A.; Thibault-Starzyk, F. Probing Zeolites by Vibrational Spectroscopies. *Chemical Society Reviews*. 2015, pp 7262–7341. https://doi.org/10.1039/c5cs00396b.

(51) Aloise, A.; Marino, A.; Dalena, F.; Giorgianni, G.; Migliori, M.; Frusteri, L.; Cannilla, C.; Bonura, G.; Frusteri, F.; Giordano, G. Desilicated ZSM-5 Zeolite: Catalytic Performances Assessment in Methanol to DME Dehydration. *Microporous Mesoporous Mater.* **2020**, *302* (March), 110198. https://doi.org/10.1016/j.micromeso.2020.110198.

(52) Jin, Z.; Liu, S.; Qin, L.; Liu, Z.; Wang, Y.; Xie, Z.; Wang, X. Methane Dehydroaromatization by Mo-Supported MFI-Type Zeolite with Core–Shell Structure. *Appl. Catal. A Gen.* **2013**, *453*, 295–301. https://doi.org/10.1016/j.apcata.2012.12.043.

(53) Bae, Y.-S.; Yazaydın, A. O.; Snurr, R. Q. Evaluation of the BET Method for Determining Surface Areas of MOFs and Zeolites That Contain Ultra-Micropores. *Langmuir* **2010**, *26* (8), 5475–5483. https://doi.org/10.1021/la100449z.

(54) Li, M.; Hu, Y.; Fang, Y.; Tan, T. Coating Mesoporous ZSM-5 by Thin Microporous Silicalite-1 Shell: Formation of Core/Shell Structure, Improved Hydrothermal Stability and Outstanding Catalytic Performance. *Catal. Today* **2020**, *339*, 312–320. https://doi.org/10.1016/j.cattod.2019.02.041.

(55) Babu, G.P., Hedge, S.G., Kulkarny, S.B., R. P. Active Centres over HZSMS Zeolites I. Xylene Isomerization. *J. Catal.* **1983**, *477*, 471–477.

TABLES CAPTIONS

Table 1. Textural properties of parent (ZSM-5_P), single- step Silicalite-1 layered catalyst (ZSM-5_X) and double-step Silicalite-1 layered catalyst (ZSM-5_XX) determined by N_2 physisorption analysis at -196°C.

Table 2. Acidity of parent (ZSM-5_P), single- step Silicalite-1 layered catalyst (ZSM-5_X) and double-step Silicalite-1 layered catalyst (ZSM-5_XX) measured by NH_3-TPD analysis and FTIR using pyridine as a probe molecule. (Data are ± Standard deviation)

Table 3. Coke formation on used parent (ZSM-5_P), single- step Silicalite-1 layered catalyst (ZSM-5_X) and double-step Silicalite-1 layered catalyst (ZSM-5_XX) after 5h time-on-stream.

FIGURES CAPTIONS

Figure 1. XRD patterns of parent (ZSM-5_P), single- step Silicalite-1 layered catalyst (ZSM-5_X) and double-step Silicalite-1 layered catalyst (ZSM-5_XX). Reference pattern is extracted from International Zeolite Association Official Structures Database (http://www.iza-structure.org/databases/) and it refers to calcined ZSM-5

Figure 2. N_2 sorption isotherms of parent (ZSM-5_P), single- step Silicalite-1 layered catalyst (ZSM-5_X) and double-step Silicalite-1 layered catalyst (ZSM-5_XX).

Figure 3. TEM pictures of parent zeolite (ZSM-5_P) showing the clean edges of (A, B) two crystals at the same magnification, M=30 nm.

Figure 4. TEM pictures of single-deposition step Silicalite-1 layered catalyst ZSM-5_X showing (A) the crystalline ZSM-5_P covered by amorphous silica particles and (B) the edge of ZSM-5_P covered by random amorphous silica particles at the same magnification, M=20 nm.

Figure 5. TEM pictures of double-deposition step Silicalite-1 layered catalyst ZSM-5_XX showing (A) the multi-Silicalite-1 layer, M=30 nm and (B) the crystalline nature of Silicalite-1 with crystalline fringes corresponding to the MFI type structure, M=50 nm.

Figure 6. NH_3-TPD profiles of parent (ZSM-5_P), single- step Silicalite-1 layered catalyst (ZSM-5_X) and double-step Silicalite-1 layered catalyst (ZSM-5_XX).

Figure 7. FTIR spectra on the parent ZSM-5_P, single-Silicalite-1 layer catalyst ZSM-5_X and multi-Silicalite-1 layer catalyst ZSM-5_XX. Left: OH-region before and after Pyridine adsorption; right: Pyridine adsorption region.

Figure 8. Methanol conversion and selectivity of parent (ZSM-5_P), single- step Silicalite-1 layered catalyst (ZSM-5_X) and double-step Silicalite-1 layered catalyst (ZSM-5_XX). Reaction condition: atmospheric pressure, WHSV=$4g_{MeOH}\cdot(g_{cat}\cdot h)^{-1}$, N_2 carrier gas.

Figure 9. Olefins formation as a function of temperature on parent (ZSM-5_P), single- step Silicalite-1 layered catalyst (ZSM-5_X) and double-step Silicalite-1 layered catalyst (ZSM-5_XX). (160-200°C; atmospheric pressure: WHSV: $4g_{MeOH}\cdot(g_{cat}\cdot h)^{-1}$, N_2 carrier gas)

Figure 10. Turn Over Frequency (TOF) of parent (ZSM-5_P), single- step Silicalite-1 layered catalyst (ZSM-5_X) and double-step Silicalite-1 layered catalyst (ZSM-5_XX).

Figure 11. GC-MS analysis of the spent parent (ZSM-5_P), single- step Silicalite-1 layered catalyst (ZSM-5_X) and double-step Silicalite-1 layered catalyst (ZSM-5_XX), revealing the presence of pentamethyl benzene and hexamethyl benzene.

Catalyst	Si/Al_{bulk} mol/mol	S_{BET}[a] (m^2/g)	S_{micro}[b] (m^2/g)	S_{ext}[b] (m^2/g)	V_p[c] (cm^3/g)	V_{micro}[b] (cm^3/g)
ZSM-5_P	15.4	404	310	94.3	0.21	0.12
ZSM-5_P_X	17.6	349	267	80.0	0.17	0.10
ZSM-5_P_XX	27.1	389	293	96.0	0.20	0.11

[a]Calculated by the multipoint BET method in the Rouquerol p/p^0 range; [b]Calculated by the t-plot method; [c]Calculated at p/p^0 0.95

Table 1

Catalyst	NH_3-TPD ($\mu mol_{NH_3}/g_{cat}$)			Py FT-IR ($\mu mol_{Py}/g_{cat}$)		
	l[a]	m[a]	**Total**	B [b]	L [b]	**Total**
ZSM-5_P	259 ± 25 (279)	424 ± 42 (456)	**683 ± 65**	446 ± 32	247 ± 2	**693 ± 34**
ZSM-5_P_X	207 ± 19 (295)	299 ± 32 (462)	**506 ± 10**	403 ± 20	232 ± 22	**635 ± 2**
ZSM-5_P_XX	195 ± 20 (272)	324 ± 35 (443)	**519± 56**	276 ± 5	183 ± 55	**459 ± 51**

[a] *l and m are low and medium temperature desorption peaks respectively. Values into parenthesis (°C);*

[b] *B: Brønsted acid sites ($IMEC_B$= 1.02 cm/µmol); L: Lewis acid sites ($IMEC_L$= 0.89 cm/µmol)*

Table 2

Catalyst	mg_{COKE}/g_{Cat}	$mg_{COKE}/g_{Formed\ DME}$
ZSM-5_P	31	0.8
ZAM-5_X	39	1.3
ZSM-5_XX	22	0.7

Table 3

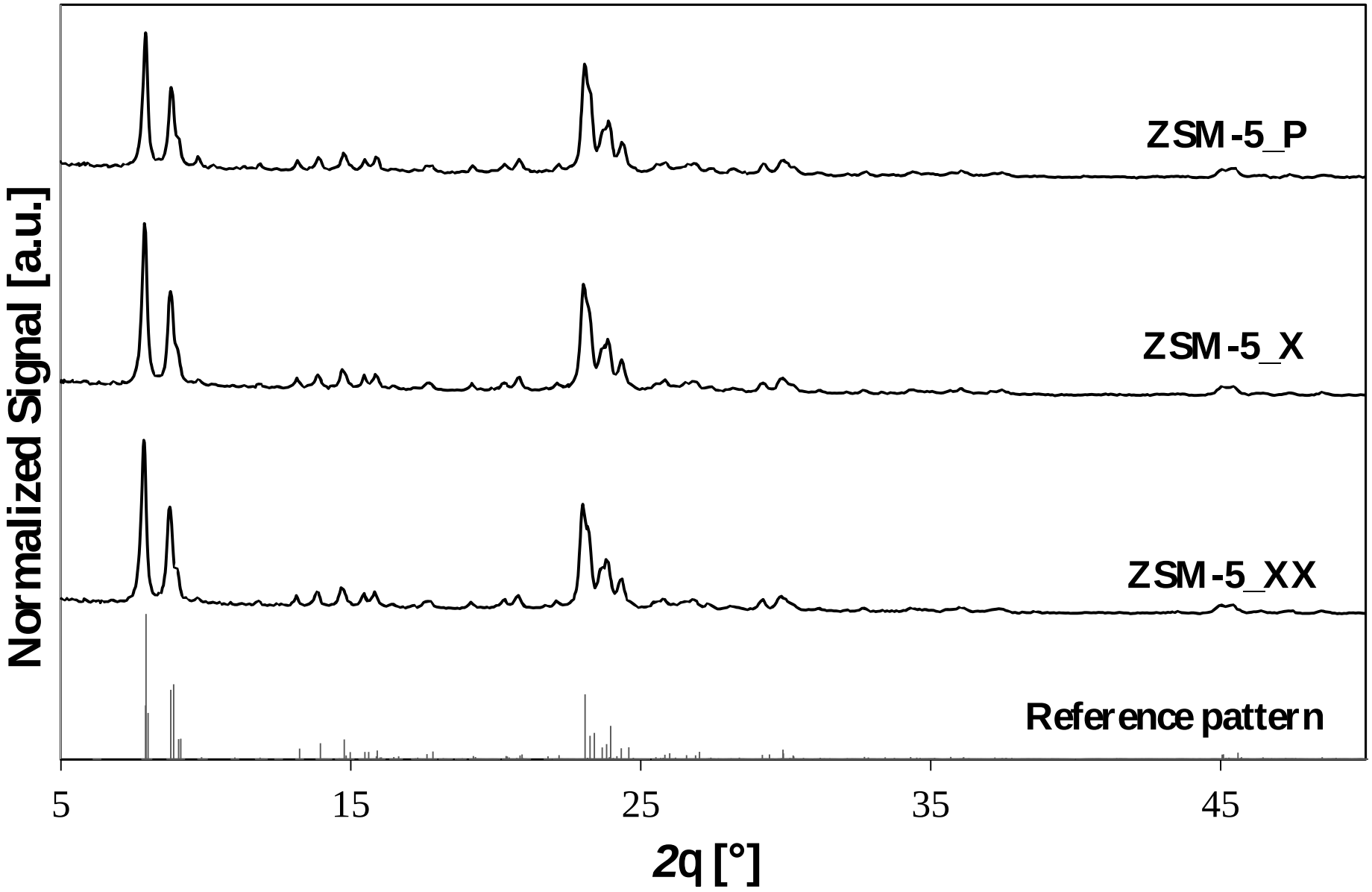
ZSM-5_P
ZSM-5_X
ZSM-5_XX
Reference pattern
Normalized Signal [a.u.]
5
15
25
35
45
2q [°]

Figure 1

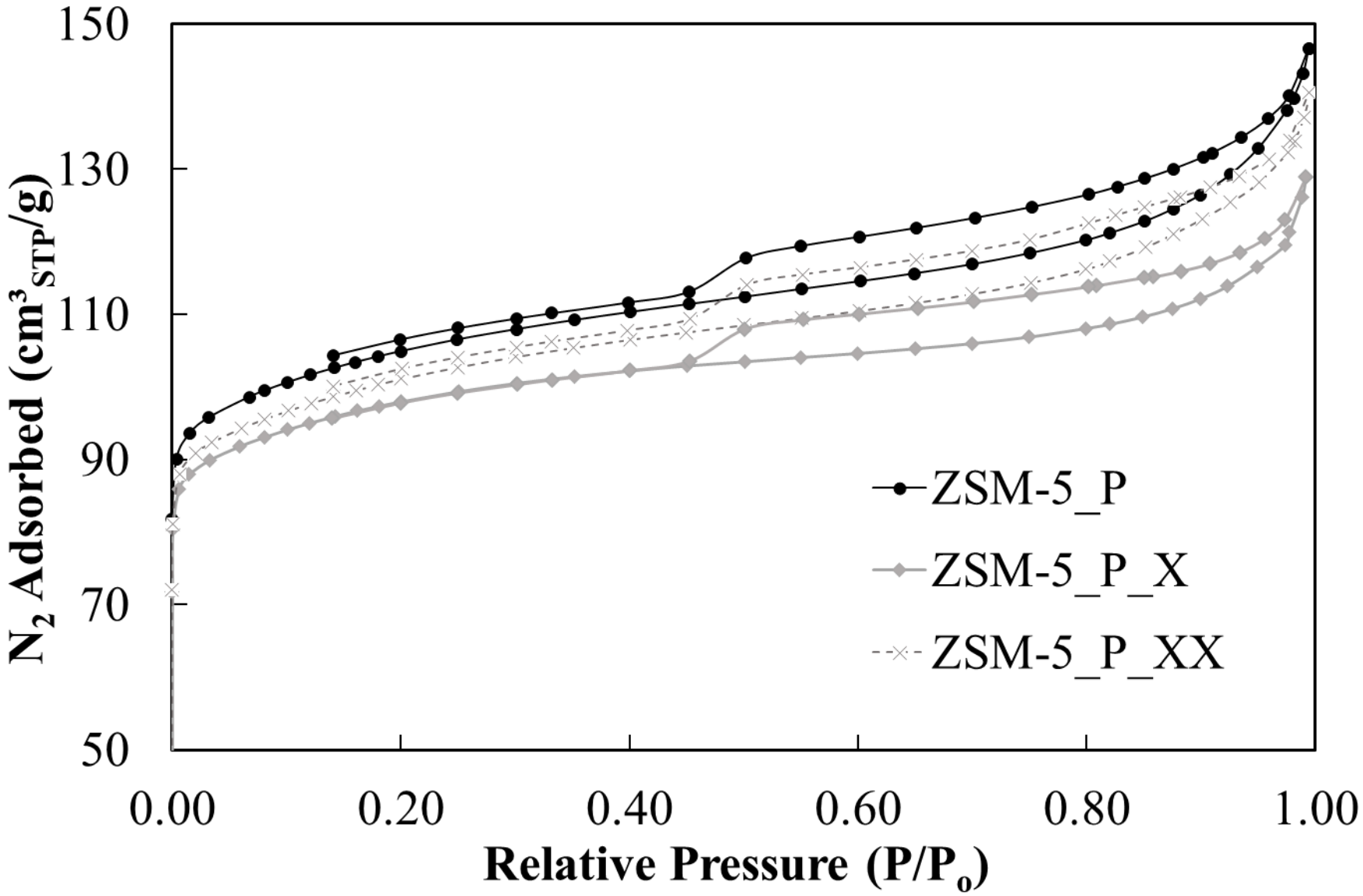
150
130
110
90
70
50
0.00
0.20
0.40
0.60
0.80
1.00
N2 Adsorbed (cm3STP/g)
Relative Pressure (P/Po)
ZSM-5_P
ZSM-5_P_X
ZSM-5_P_XX

Figure 2

Figure 3

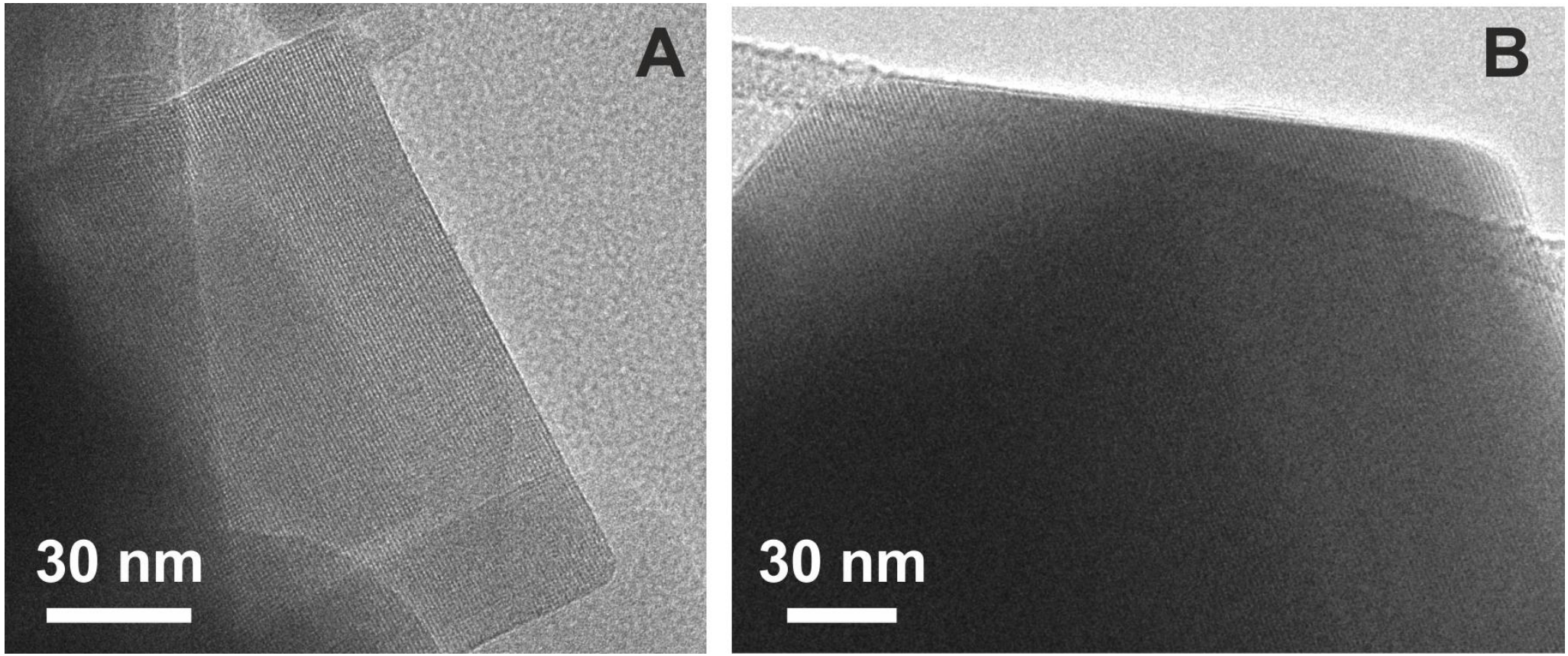

Figure 4

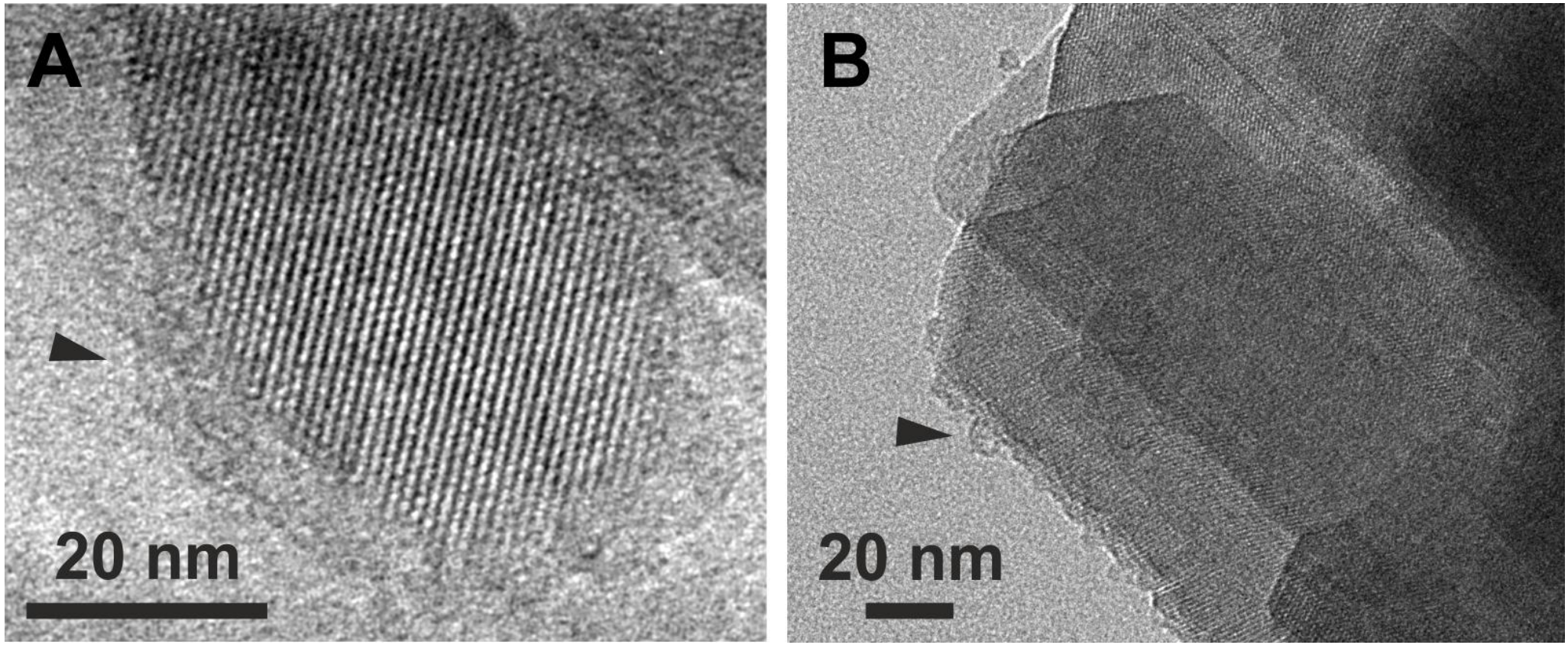

Figure 5

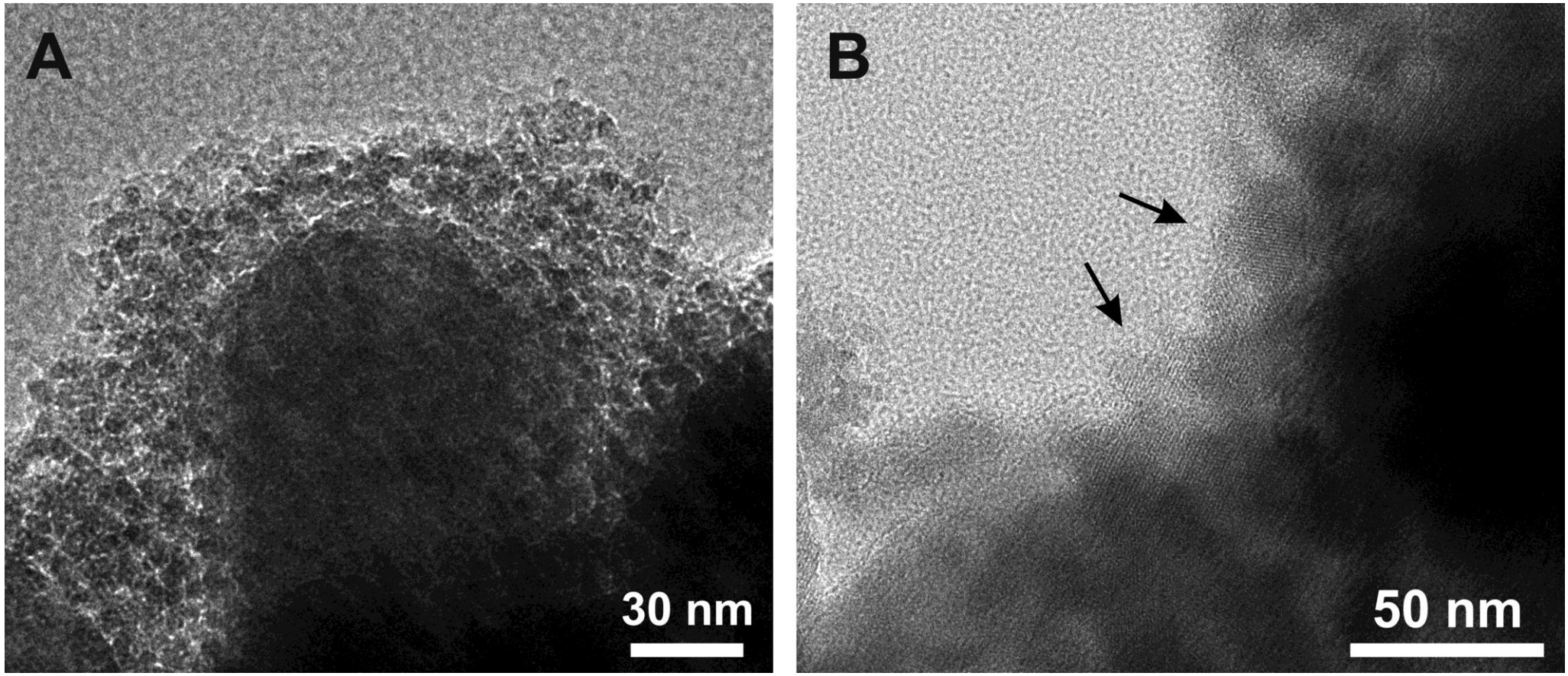

Figure 6

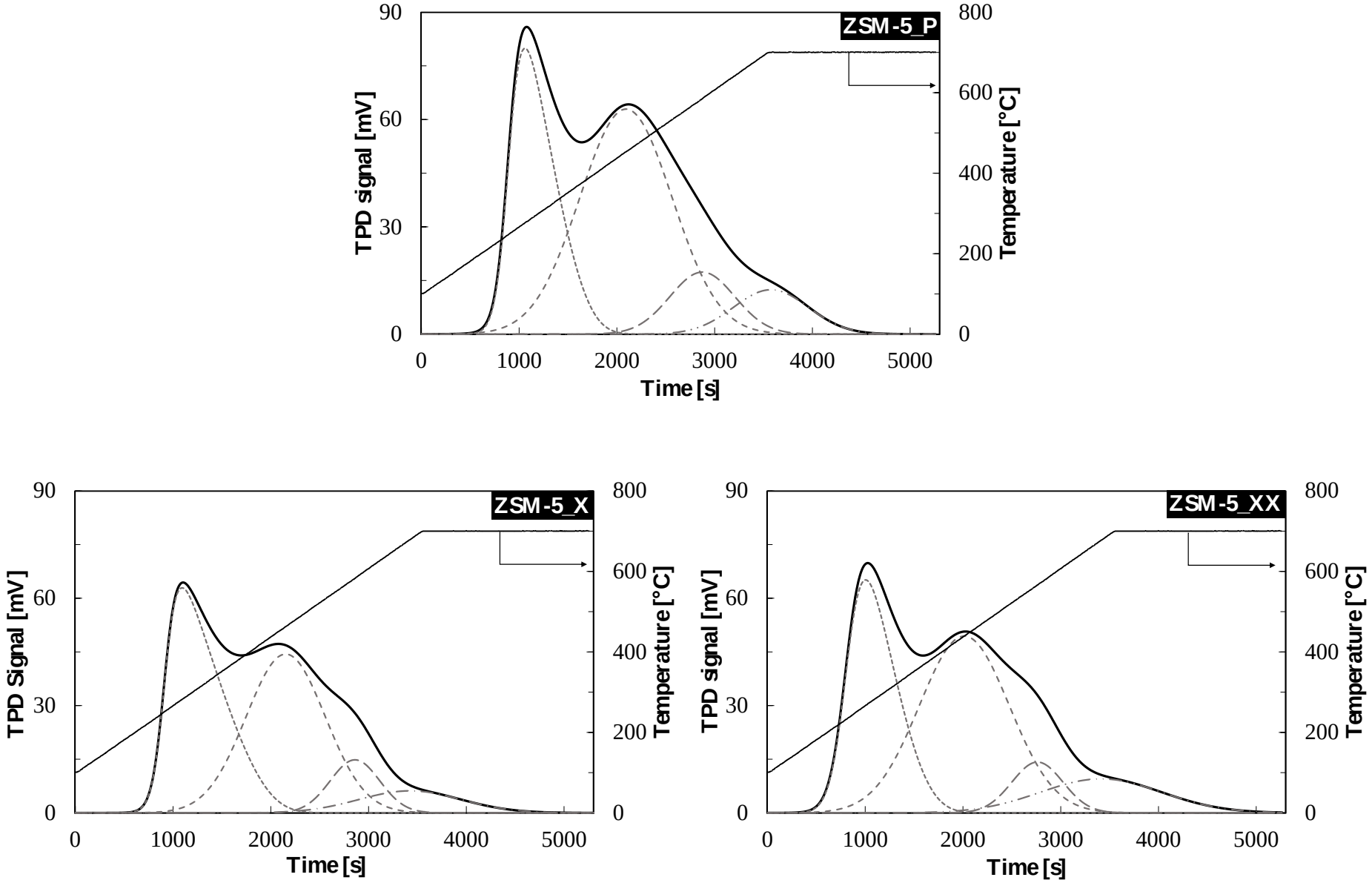
ZSM-5_P
TPD signal [mV]
Temperature [°C]
Time [s]
0
30
60
90
200
400
600
800
1000
2000
3000
4000
5000
ZSM-5_X
TPD Signal [mV]
ZSM-5_XX

Figure 7

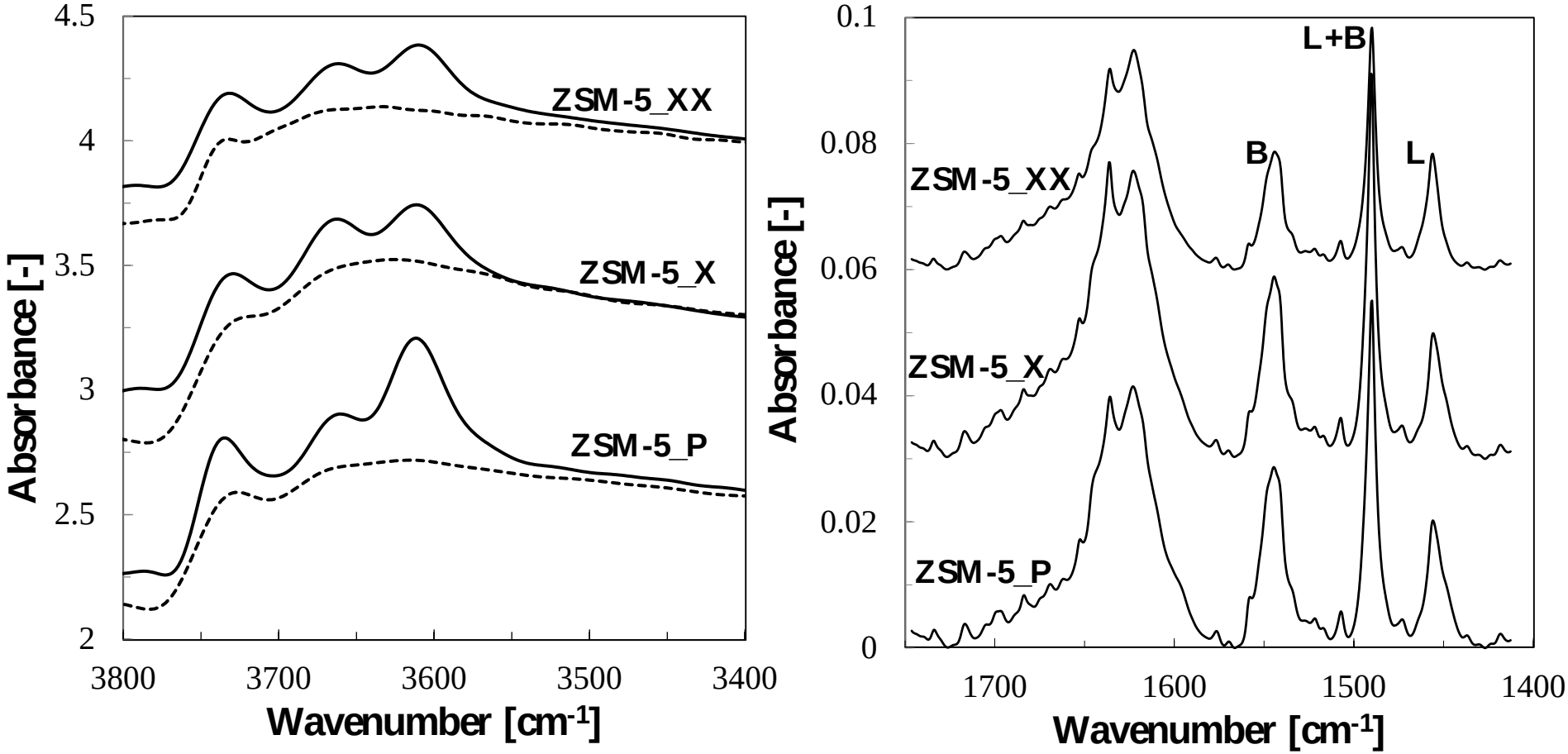
4.5
4
3.5
3
2.5
2
Absorbance [-]
ZSM-5_XX
ZSM-5_X
ZSM-5_P
3800
3700
3600
3500
3400
Wavenumber [cm-1]
0.1
0.08
0.06
0.04
0.02
0
Absorbance [-]
L+B
B
L
ZSM-5_XX
ZSM-5_X
ZSM-5_P
1700
1600
1500
1400
Wavenumber [cm-1]

Figure 8

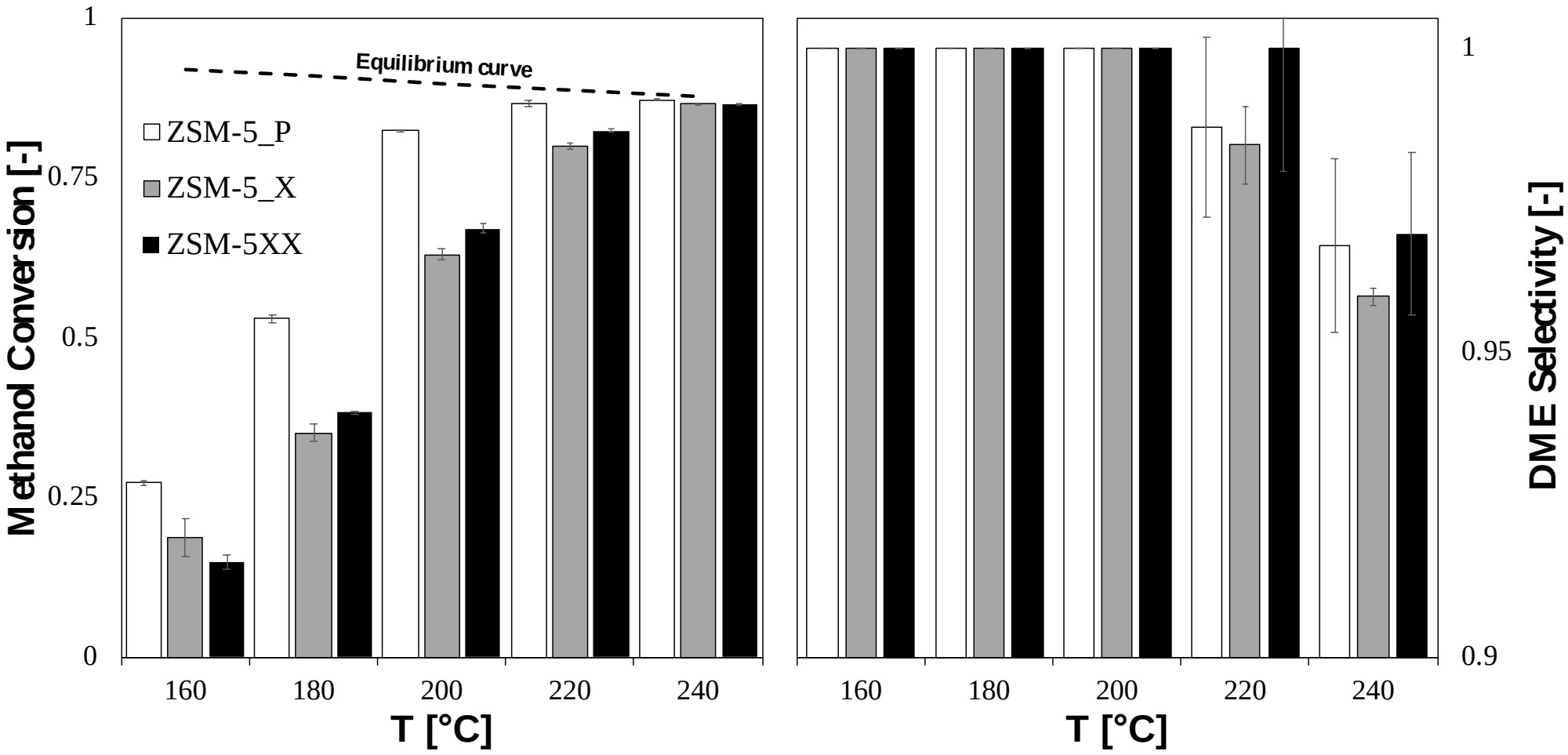
Equilibrium curve
ZSM-5_P
ZSM-5_X
ZSM-5XX
Methanol Conversion [-]
DME Selectivity [-]
T [°C]
T [°C]
0
0.25
0.5
0.75
1
0.9
0.95
160
180
200
220
240

Figure 9

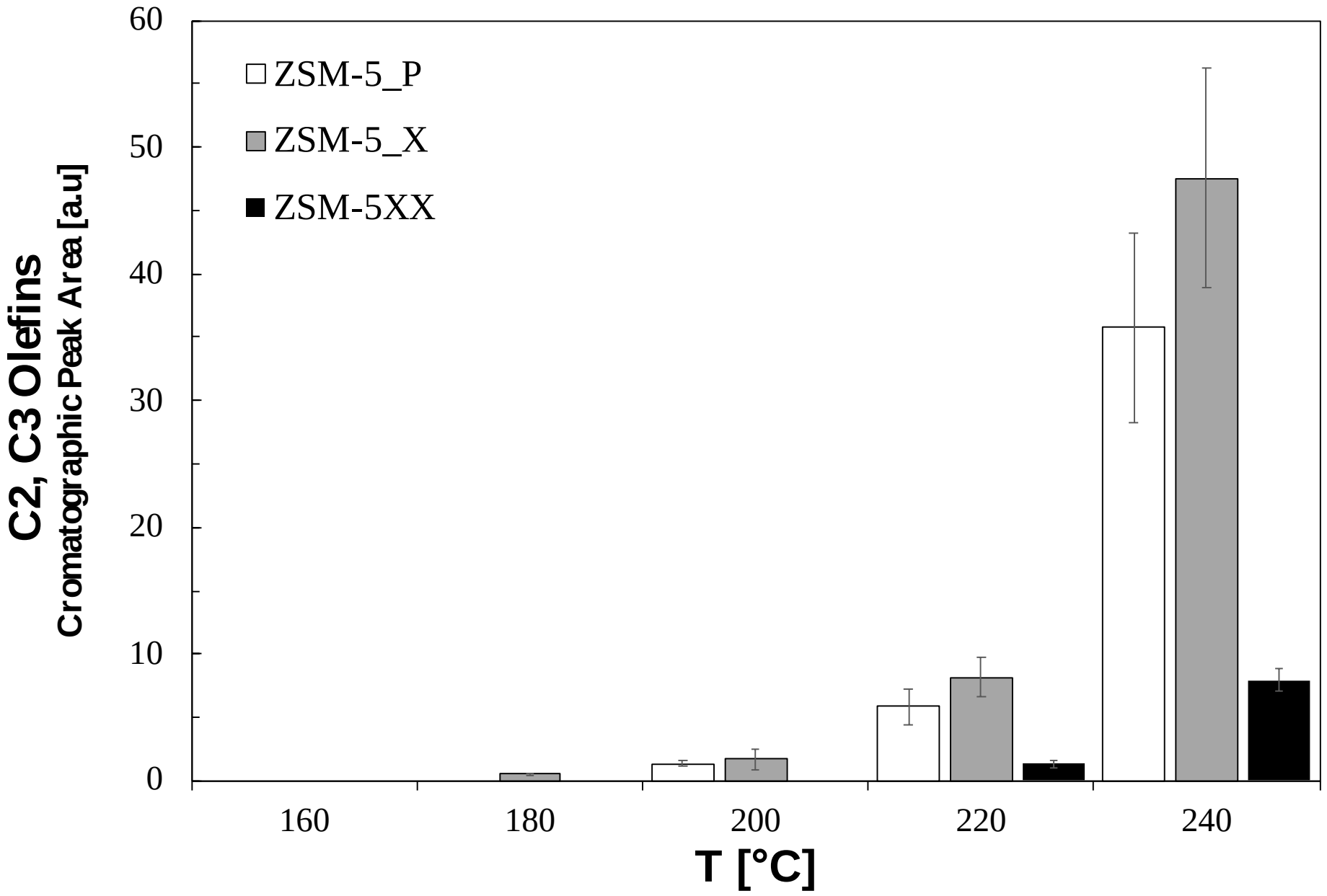
ZSM-5_P
ZSM-5_X
ZSM-5XX
C2, C3 Olefins
Cromatographic Peak Area [a.u]
60
50
40
30
20
10
0
160
180
200
220
240
T [°C]

Figure 10

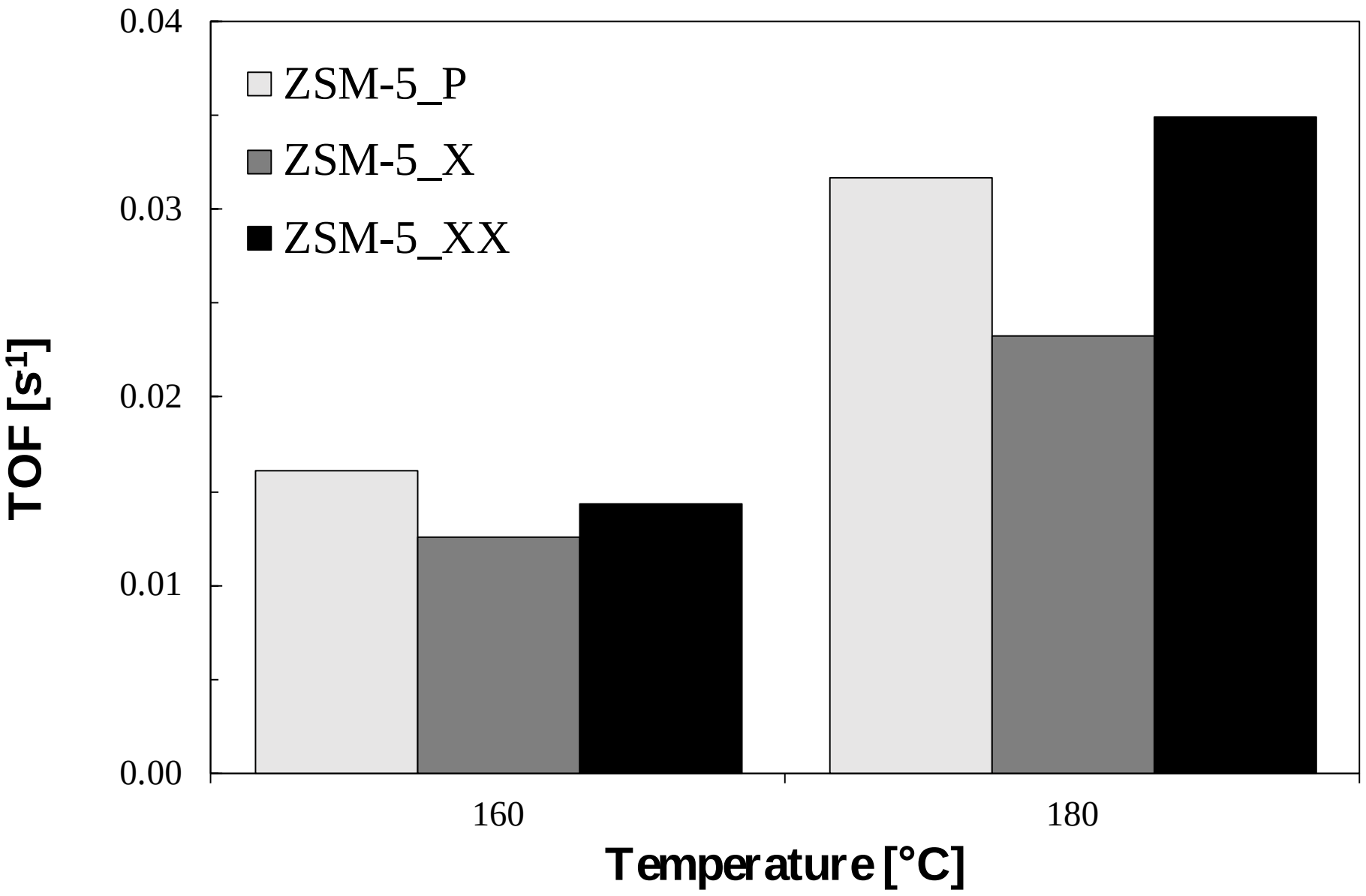
0.04
0.03
0.02
0.01
0.00
ZSM-5_P
ZSM-5_X
ZSM-5_XX
TOF [s-1]
160
180
Temperature [°C]

Figure 11

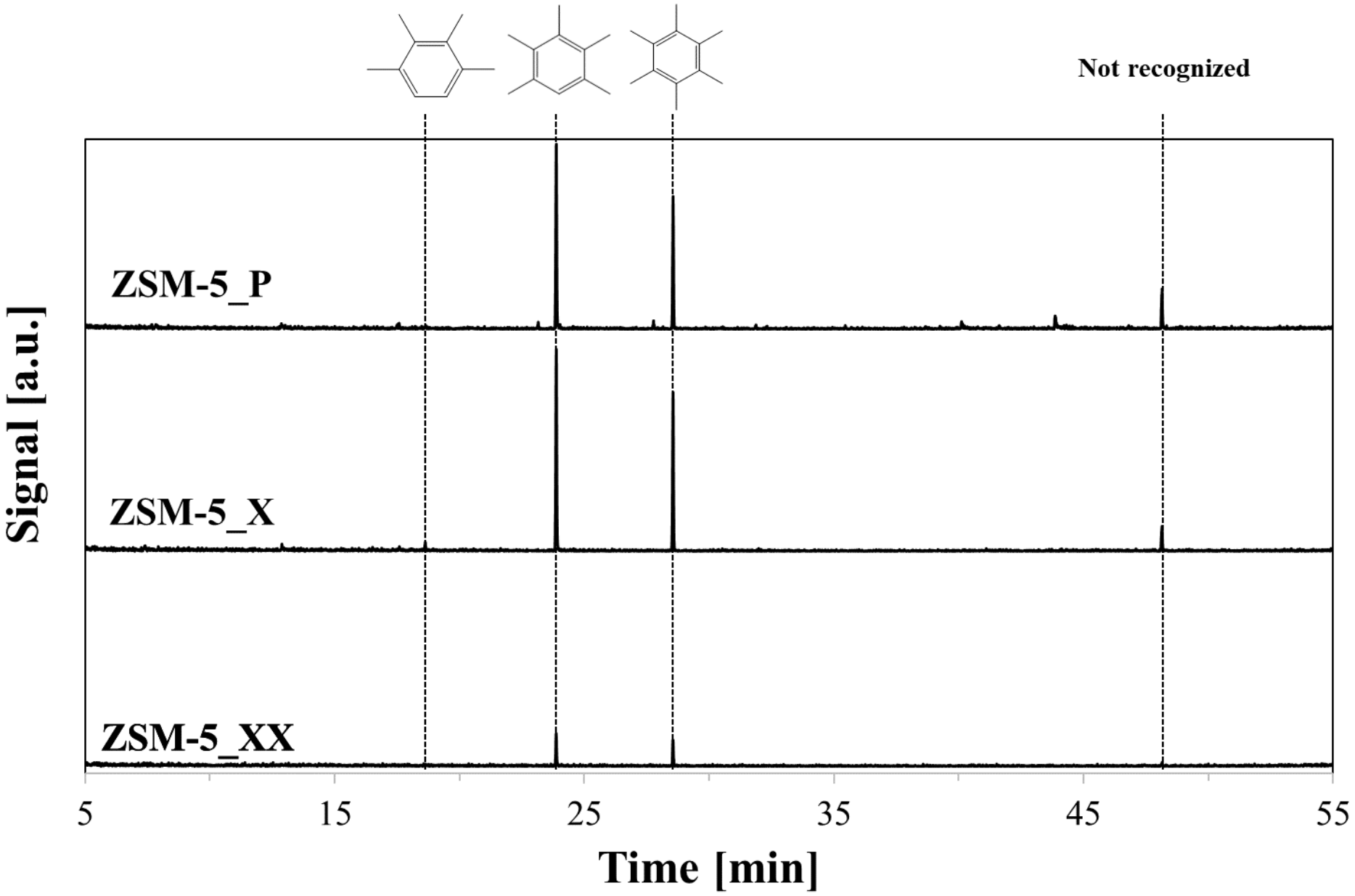
Not recognized
ZSM-5_P
ZSM-5_X
ZSM-5_XX
Signal [a.u.]
5
15
25
35
45
55
Time [min]

Figure 12